



Distortional buckling behavior and design consideration of castellated beams considering residual stresses

Xuhong Zhou¹, Ziqi He², Peng Chen³, Jingchao Li⁴, Zhanjie Li⁵

Abstract

This work will focus on the distortional buckling behavior of castellated beams with the related design consideration of moment gradient factor and residual stress. With the limited studies on the distortional buckling behavior of castellated beams and a lack of design recommendations, there necessitates more studies related to this behavior of the beams. Firstly, an experimental investigation on the distortional buckling of castellated beams fabricated from two hot-rolled parent profiles is briefly introduced in this study. The distortional buckling behaviors of the castellated beam was carefully measured and analyzed. Based on the test results, the design consideration of the moment gradient factor was discussed. To examine the influence of the fabrication procedure on the residual stress pattern, the residual stresses were measured in a number of castellated member specimens and their parent sections. These measured residual stresses demonstrated the distribution of the residual stresses in the castellated beam sections and provide a data set for future validation of computational simulation of the residual stress pattern for design recommendation.

1. Introduction

Castellated beams are commonly manufactured by cutting the web of an I-beam or H-beam along a predefined line (e.g., a zigzag line) and then welding the halves following a certain pattern. Compared with their parent I-section (or H-section) beams, castellated beams possess distinct merits in terms of a lighter weight, greater flexural stiffness, better aesthetic architectural appearance, and substantial material efficiency, etc. Hence, castellated beams are widely used in stadiums, large-span bridges, plants, and multi-story buildings. This stems a broad research of their behaviors over the last few decades. In particular, different failure modes of castellated beams were identified including the flexural failure (Toprac & Cooke 1959), the shear or vierendeel collapse mechanism (Altifillisch et al. 1957; Toprac & Cooke 1959), the rupture of welded joints (Husain & Speirs 1973), the buckling of web post (Zaarour & Redwood 1996), the lateral-torsional buckling (Kerdal & Nethercot 1984; Nethercot & Kerdal 1982), and the distortional buckling (Ellobody 2011; Zirakian & Showkati 2006). The last failure mode is

¹ Professor, Chongqing University, <zhouxuhong@126.com>

² Associate Professor, Chongqing University, <heziqu@cqu.edu.cn>

³ Ph.D. student, Chongqing University, <cp12051@cqu.edu.cn >

⁴ Ph.D. student, Hunan University, <jingchao1028@163.com>

⁵ Assistant Professor, SUNY Polytechnic Institute, <zhanjie.li@sunypoly.edu>

relatively complex; especially it can be potentially coupled with local and/or lateral-torsional buckling.

In general, compared with their parent beams, castellated beams are more susceptible to failure mode of distortional buckling due to the effect of residual stresses developed in the fabrication process, geometric imperfections such as mismatch between the upper and lower halves, and large slenderness of the web. The typical distortional failure modes of castellated beams are shown in Fig. 1. For castellated beams of intermediate length with stocky flanges and slender webs, the buckling mode is usually characterized by combined lateral displacement and twist along with localized distortions of the web, as shown in Fig. 1. This mode possesses the coupling behavior with lateral-torsional buckling. If restraints are applied to the tensile side of the flange, the restrained distortional buckling as shown in Fig. 1b may occur.

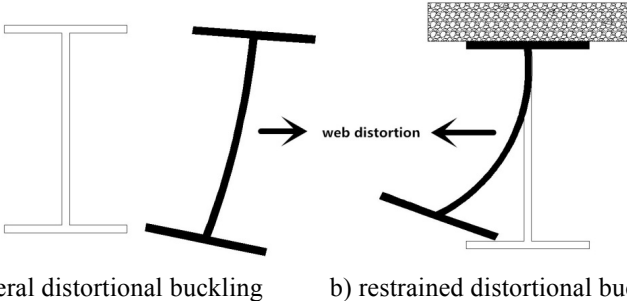


Figure 1: Distortional buckling modes: (a) lateral distortional buckling; (b) restrained distortional buckling

A large amount of researches has been conducted on the distortional buckling mode of the steel I-section beams both experimentally and numerically. For instances, (Bradford 1992) summarized the extensive studies of the web distortion effects on the lateral buckling of I-beams. (Pi & Trahair 2000) investigated the distortional buckling of doubly symmetric I-sections and proposed design expressions of calculating the elastic distortional buckling moment due to the web distortion. (Kalkan & Buyukkaragoz 2012) also developed analytical expressions applicable to elastic and inelastic lateral distortional buckling of doubly symmetric I-beams. (Zirakian 2008) and (Zirakian & Showkati 2007) conducted an experimental study to investigate the distortional buckling of doubly symmetric I-beams and compared with the code predictions.

Meanwhile, compared to ordinary steel I-beams, there were fewer studies on the distortional buckling behavior of castellated beams. The only experimental studies available so far are conducted by (Zirakian & Showkati 2006) and (Showkati et al. 2012). In (Zirakian & Showkati 2006) the lateral and restrained distortional buckling of castellated beams were experimentally studied on six full-scale castellated beams. While in (Showkati et al. 2012), the focuses was to investigate the effect of elastic bracing on the load resistance of castellated beams when failed by lateral buckling accompanied with web distortion. Numerically, (Ellobody 2011) investigated the combined lateral-torsional and distortional buckling behavior of castellated beams with a parametric study to analyze the influencing factors and evaluate the application of specification predictions. Other numerical investigations in (El-Sawy et al. 2014; Mohebkhah 2004; Sweedan 2011) are available in assessing the influence of various geometrical parameters on the elastic and inelastic stability of castellated and cellular beams.

With the limited studies on the distortional buckling behavior of castellated beams and a lack of design recommendations, there necessitates more studies related to this behavior of the beams. In this paper, six full-scale castellated beams, which are laterally braced at the end supports and at the upper flange in the mid-span, are loaded at the mid-span to investigate the distortional buckling behaviors. The web distortions at one-quarter span and the mid-span are measured and analyzed. Furthermore, for the purpose of future computational simulations, their associated residual stresses are experimentally measured and distributions with the cross section and the beam are presented. Future work for a comprehensive design recommendation is discussed.

2. Experimental test of castellated beams

2.1 Test specimens

The tested castellated steel beams were fabricated from two types of hot-rolled parent profiles HN200*100 and HN250*125 in the Chinese Standard of GB/T11263-2010 (GB/T11263-2010). The steel has an average yielding stress of 280 MPa and ultimate stress of 435 MPa from coupon tests. In general, lateral distortional buckling may typically occur in the intermediate length of castellated beams with stocky flanges and slender webs, and additionally in order to investigate the influence of the moment gradient factor C_b of castellated beams experiencing distortional buckling, beams of each cross-sectional type were manufactured with three different lengths. The nominal and actual cross-sectional dimensions of castellated beams used in tests are tabulated in Table 1 according to a preliminary finite element analysis of each specimen to determine the lengths that may have a large web distortion. The geometry of the section is shown in Fig. 2. Note that there are some differences between the nominal and actual values.

Table 1: Dimensions of test beams.

Test beam ^a	H (mm)		B (mm)		t_w (mm)		t_f (mm)		L^b (mm)	n^c
	Nominal	Actual	Nominal	Actual	Nominal	Actual	Nominal	Actual		
JA-L16	297	296	99	98	4.5	4.9	7	6.0	4752	16
JA-L18	297	295	99	101	4.5	4.8	7	6.0	5346	18
JA-L20	297	295	99	101	4.5	4.8	7	6.2	5940	20
JB-L16	372	370	124	125	5	5.3	8	6.9	5952	16
JB-L18	372	372	124	125	5	5.0	8	6.9	6696	18
JB-L20	372	372	124	124	5	5.3	8	6.9	7440	20

^aThe “J” stands for distortional buckling, “A” - HN200*100 and “B” - HN250*150 stand for type of the section, “L16”, “L18” and “L20” stand for number of holes along the length.

^bThe “L” stands for the distance between the end supports.

^cThe “n” stands for number of holes along the length.

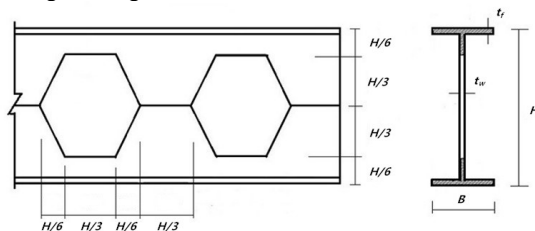


Figure 2: Illustrated geometrical parameters of the specimens

2.2 Experimental program

The test setup is illustrated in Fig. 3. The load was centrally located in the mid-span of the beam. The beam is simply supported with lateral bracing at the end supports as well as at the mid-span of the upper flange.

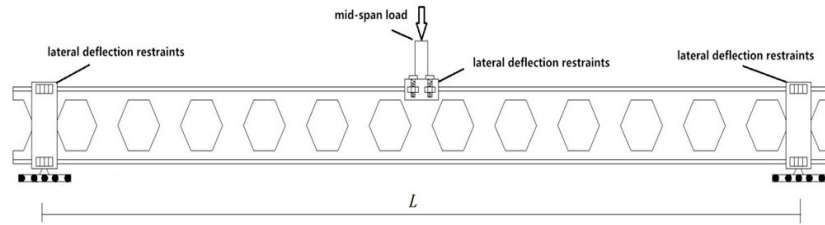


Figure 3: Test setup

The lateral displacements and twists at both end supports of the specimens were fully restricted by the lateral restraint, which consisted of four ball bearings tied to the two supporting columns and tightly attached to both sides of the specimens, as shown in Fig. 4a and 4b. The detail of the loading frame is demonstrated in Fig. 4c. There were four pulleys at the corners of the loading frame, which could be adjusted horizontally and kept in close contact with the reaction columns, thus the lateral movement of the loading frame would be avoided. Through a manually operated hydraulic jack fixed on the reaction columns, the loading frame could be pushed down vertically. To reduce the effect of eccentricity, two load cells arranged symmetrically on both sides of the beams were used during the experiments. The lateral deflection of the top flange at the mid-span was effectively restricted by the loading plate through friction as well as four bolts fixed on the loading plate.

It was expected that the lateral-distortional buckling (Fig. 1a) would occur in the two laterally un-braced spans between the end support and the loading point at the mid-span, and the restrained distortional buckling (Fig. 1b) would occur around the mid-span. Hence, lateral deflections, vertical displacements as well as web transverse strains were monitored at the 1/4 and 1/2 span of the beam as shown in Fig. 5. Two strain gauges were arranged at the mid-height of both sides of the web to record the transverse strains.

In the tests, to record the web distortion at the 1/4 span of the beam, lateral deflections at the top flange, 3/4 point, mid-point, 1/4 point, and bottom flange levels of the section height were measured using five displacement transducers with a capacity of 30 mm. The displacement transducers were fixed on a board, which was in a plane perpendicular to the web and located 3000 mm away from the beams, as shown in Fig. 6a. At the 1/2 span of the beams, as the lateral deflection of the top flange was effectively restricted by the loading plate and bolts, the lateral deflections were measured at four points through four displacement transducers fixed on the loading frame, as shown in Fig. 6b. The vertical displacements at the 1/4 span were recorded using the displacement transducers which were attached on the frame by steel angle, while the vertical displacements at mid-span were measured by displacement transducer fixed on the loading frame directly, as shown in Fig. 7. The dynamic signal testing and analyzing system was employed to monitor and record the developed displacements, strains, as well as the applied load throughout the tests.

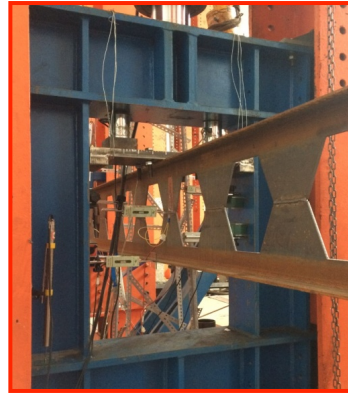
Consistent with the common practice of all the tests, as the first stage of the test, a preliminary load was applied to check the readings of instrumentations and then unloaded. Thereafter, the load was applied in a step-by-step manner until the lateral buckling of the laterally unsupported spans could be obviously observed. Meanwhile, the deflections and strains of the specimen were recorded by their measuring devices at a very short interval throughout the experiments.



(a) overall view of the test

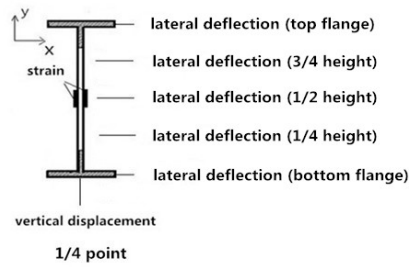


(b) end support lateral restraints

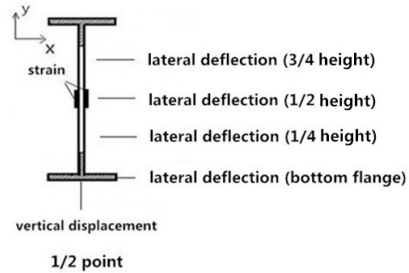


(c) loading point restraints

Figure 4: Test setup: (a) overall view of the test; (b) end support lateral restraints; (c) loading point restraints.



(a) 1/4 span



(b) 1/2 span

Figure 5: Diagrammatic sketch of displacement and strain measurements: (a) 1/4 span; (b) 1/2 span



(a) displacement transducer at 1/4 span



(b) displacement transducer at 1/2 span

Figure 6: Detailed lateral deflections measurement



(a) displacement transducer at $\frac{1}{4}$ span (b) displacement transducer at $\frac{1}{2}$ span
Figure 7: Vertical displacements measurement at $\frac{1}{4}$ and $\frac{1}{2}$ span of the beam

2.3 Experimental results

2.3.1. Buckling deformation

In the initial stage of the experiments, the lateral and vertical deflections of the specimens increased elastically as the load increased. Deflections increased sharply once the applied load reached the values close to the critical load. Consistent with all the experimental results, the buckling mode was a full sine wave and web-post buckling did not occur in all the tested beams. Typical buckling deformation of the tested beam is shown in Fig. 8. It can be observed that the lateral deflection of the section at $\frac{1}{4}$ span were obvious and the lateral displacement of the lower flange at the mid-span can be observed clearly. The distortion of the web at the $\frac{1}{4}$ and $\frac{1}{2}$ spans could be detected through the measured lateral deflections of five points at $\frac{1}{4}$ span as well as four points at mid-span (see Fig. 6) during the loading process.

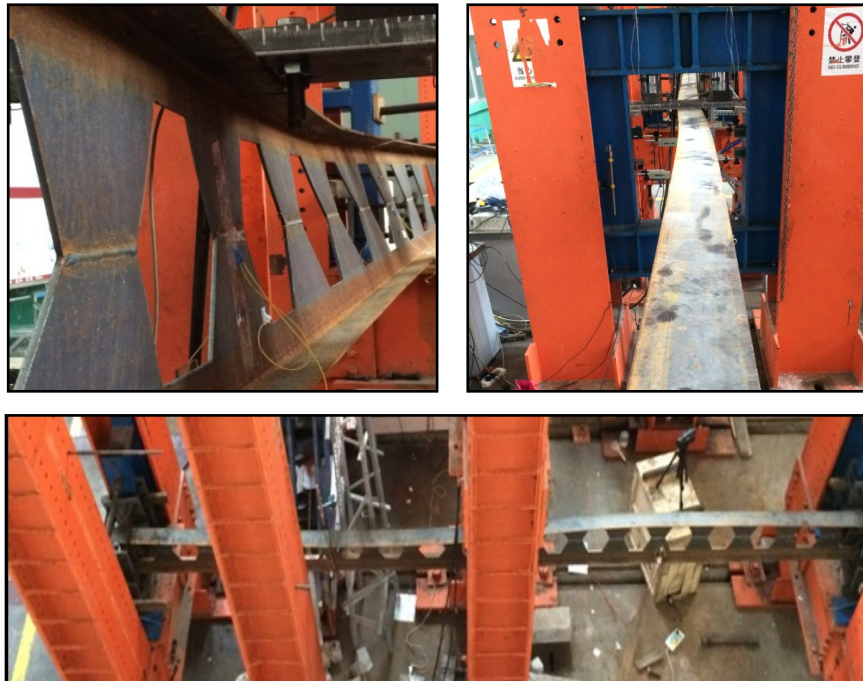


Figure 8: Distortional buckling deformation (e.g., JB-L18) from different views

2.3.2. Load responses

Typical curves of the load versus lateral deflections at the 1/4 span and 1/2 span are plotted in Figs. 9 and 10 for selected beams. First, the critical loads of the beams can be identified from these load response curves. As shown in Figures 9 and 10, the critical load is at 56 kN for the beam JB-L18 and 41 kN for the beam JA-L18. Second, the unequal divergences of the lateral displacements of the five section-height points at the 1/4 span indicates that the five points did not remain on a straight line due to the web distortion. Similar pattern also appeared in the web at the mid-span. Meanwhile, the load versus transverse strain developed at both sides of the web at the 1/4 span and mid-span are depicted in Figs. 11 and 12. The web distortion could be represented by discrepancies in the amounts of strains at mid-height on both sides of the web.

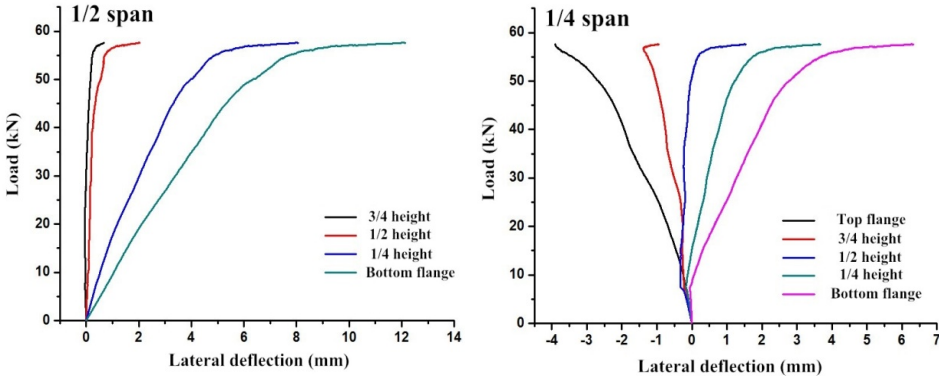


Figure 9: Load-deflection curves (JB-L18)

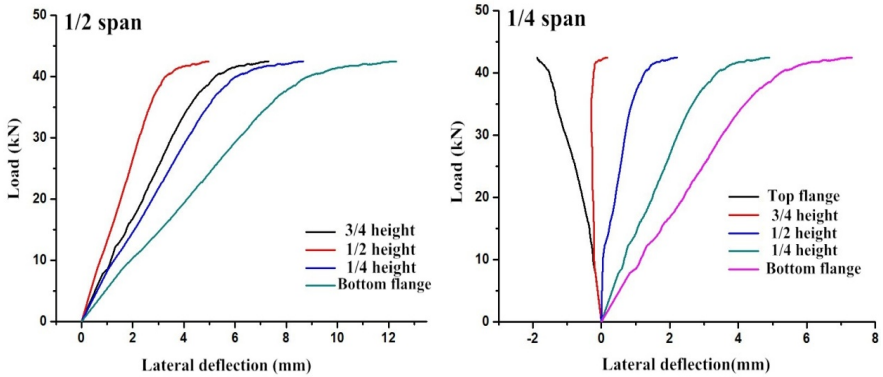


Figure 10: Load-deflection curves (JA-L18)

Through these load responses and the observed deformation during the tests, the behavior of the test castellated beams demonstrated a lateral-torsional deformation under the concentrated loading at the mid-span. Though not measured in the test, the initial imperfection of the castellated beam (usually quite big due the nature of the manufacture process) led a gradual deformation aforementioned. Also it led to distortion of the web as well and the web distortion got intensified with the increase of the load. When the load reached the critical load, this web distortion reached to its maximum magnitude accompanied with the large deflection in the unbraced bottom flange. Ultimately, the failure of the castellated beams demonstrated a lateral instability at the 1/4 spans coupled with web distortion. Consequentially, the restrained distortional and lateral-distortional buckling failures were observed at the mid-span and one-quarter span of the beams, respectively.

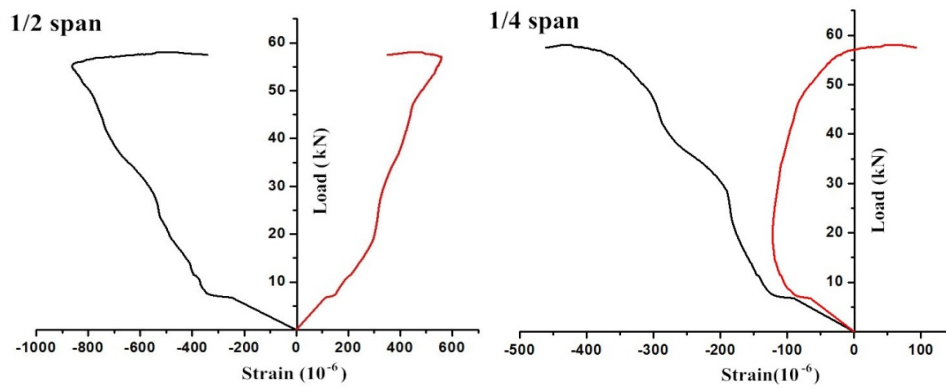


Figure 11: Load-strain curves (JB-L18)

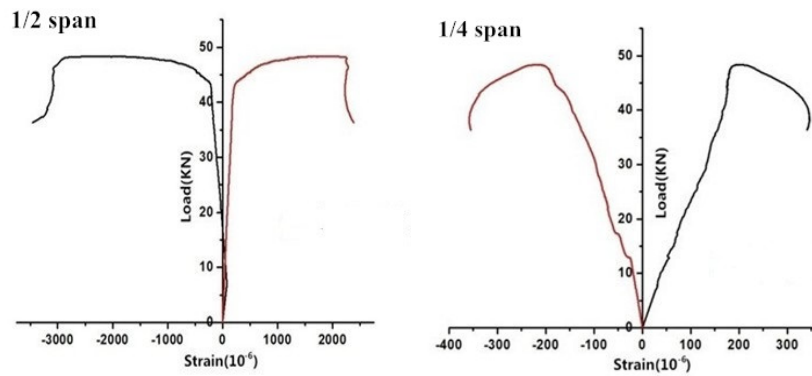


Figure 12: Load-strain curves (JA-L18)

Furthermore, based on the measured lateral deflections during the loading process, deformations of the web at 1/4 span and mid-span is illustrated in Figs. 13 and 14 for JB-L18 and JA-L20, respectively, as a demonstration. It should be noted that the evolutions of web deformation of the specimens were different among the specimens in the loading process. As shown in Figs. 13 and 14, the web deformation of JB-L18 increased gradually as the load increased, while the web deformation of JA-20 was not obvious until the concentrated load was close to the critical load. Besides the member type's influence, different initial imperfections of the tested beams may have contribution as well.

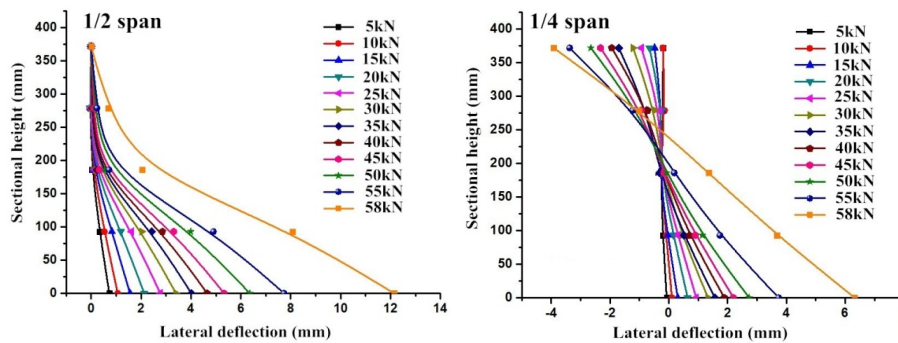


Figure 13: Deformations of the web (JB-L18) during loading

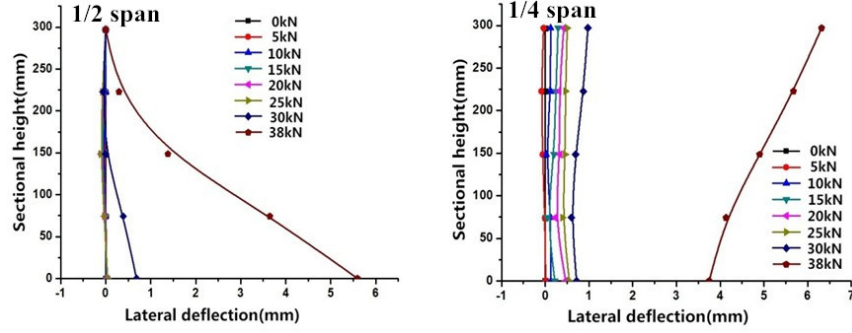


Figure 14: Deformations of the web (JA-L20) during loading.

2.3.3 The moment-gradient factor of castellated beams in distortional buckling

For beams under lateral-torsional buckling, the strength predicted under the constant moment is usually conservative. A moment gradient factor is usually adopted to take into account of the beneficial effect of the moment gradient. For instance, in AISC design specifications (AISC 2010), for loading case the same as the tested one, the moment gradient factor C_b is 1.67. This value is specified to lateral-torsional buckling, which depends only on the type of the beam and loading cases. However, failure modes also had a large impact on the C_b value as well as studied in (El-Sawy et al. 2014; Mohebkah 2004; Sweedan 2011).

The comparison of C_b values between the experimental results and the AISC is shown in Table 2 and Fig. 15. It can be found that the value of the moment gradient factor C_b is below the AISC specified. Though variation is observed among the tested beams, the variance is relatively small. A mean value of 1.49 can be obtained. Hence, reduction in the C_b value needs to be considered for castellated beams failed by lateral-distortional buckling due to the web distortion.

Table 2: C_b factors for the specimens in distortional buckling.

Specimens	P_{test}^a	P_{AISC}^b	$C_{btest} = P_{test} C_{bAISC} / P_{AISC}$	C_{bAISC}
JA-L16	48.35	53.17	1.52	1.67
JA-L18	43.01	47.94	1.50	1.67
JA-L20	38.05	44.65	1.42	1.67
JB-L16	67.50	76.74	1.47	1.67
JB-L18	58.01	67.83	1.43	1.67
JB-L20	50.78	53.17	1.59	1.67

^a P_{test} is the distortional buckling resistance of the specimens in tests.

^b P_{AISC} is the approximated distortional buckling resistance of the specimens under constant moment according to the AISC utilizing the flexural strength prediction.

3. Measurement of residual stress in castellated beams

A castellated beam is commonly produced by flame cutting the web of an I-beam (or H-beam) along with a predefined line and then welding the halves following certain pattern. During the production of the castellated beam, the intense localized heating in the cutting and welding processes causes severe thermal gradients, which result in thermal residual stresses due to the uneven cooling. Typically, the tensile residual stresses (up to the material's yield stress) are generated at the locally heated zone and balanced by the compressive stresses in the remaining portion of the beam. It is expected that this production process will significantly change the

initial residual stresses in the conventional I-beam (or H-beam). For future computational simulation and possible validation of the residual stress pattern for design recommendations, the related residual stresses of the tested beam sections were measured herein.

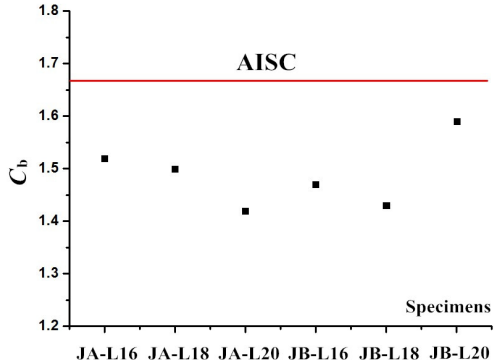


Figure 15: Comparison of C_b from experimental results and the approximated AISC method

3.1 Experimental program

Two castellated beams that have the same cross-sections as two of the tested beams: “A” - HN200*100 and “B” - HN250*150, in the previous section were manufactured using the same fabrication process as shown in (Sonck 2014). The actual cross section dimensions are HN198*99*4.5*7(A) and HN248*124*5*8 (B), respectively. Each section was fabricated 6000 mm long. For each beam, three measurements along the beam (at three different location along the beam) were taken during the fabrication process after sectioning: (1) the residual stress in the parent H beam before the fabrication; (2) the residual stress after flame cutting with a zigzag pattern; (3) the residual stress after welding, as illustrated in Fig. 16. The longitudinal residual stress was measured with using distributed strain gauges in the web and flanges using a destructive relaxation method using longitudinal cuts at each strain gauge, i.e., the sectioning method the same as (Sonck 2014). For each segment, the strain difference before and after the relaxation can be used to calculate the residual stresses. For the flange, 7 strain gauges (i.e., 7 segments) were evenly distributed as shown in Fig. 17a. For the web, the number of strain gauges used varied. For the residual stress in the parent beam, 11 strain gauges were used. After the flaming cutting, 3 strain gauges were attached in the web for measurement. Meanwhile, after the welding, 16 strain gauges were glued in the web as shown in Fig. 17b. Then, these measured strain were converted to the stress following the Hooke’s law.

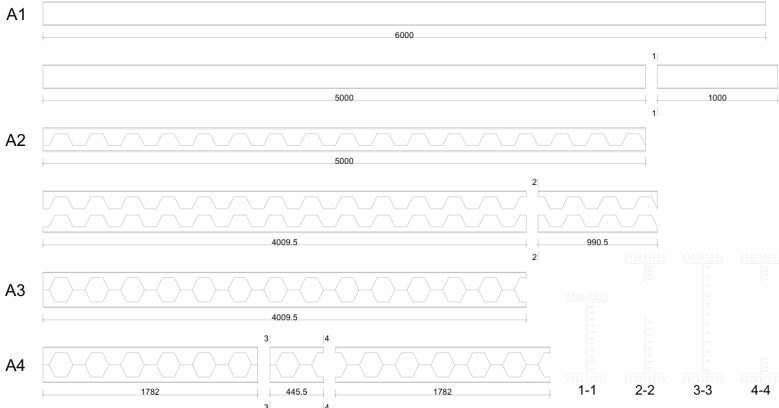


Figure 16: The residual stress measuring locations during the fabrication process



(a) the flange (b) the web after welding

Figure 17: strain gauge locations for measuring residual stresses of the casted beams

3.2 Measured residual stress

The measured residual stresses in the beams are shown in the Figs. 18 and 19 for A and B sections, respectively, for all the three measurements during the fabrication process. For both beam, the maximum residual stress in the parent section was around 60 MPa in flange and 100 MPa in the web. The sequential cutting and welding introduced more thermal residual stresses in the section. For example, the maximum flange residual stress in A section was increased to 120 Mpa at the web post section after flame cutting and welding. As can be observed from the figures, the maximum residual stress after the fabrication process is definitely section dependent as shown, for instance, the A section had a smaller maximum value than the B section. In general, the residual stress patterns of the flange and web in the web post section (c) and Tee section (d) would be highly interested for design recommendation and possible simplifications are desired.

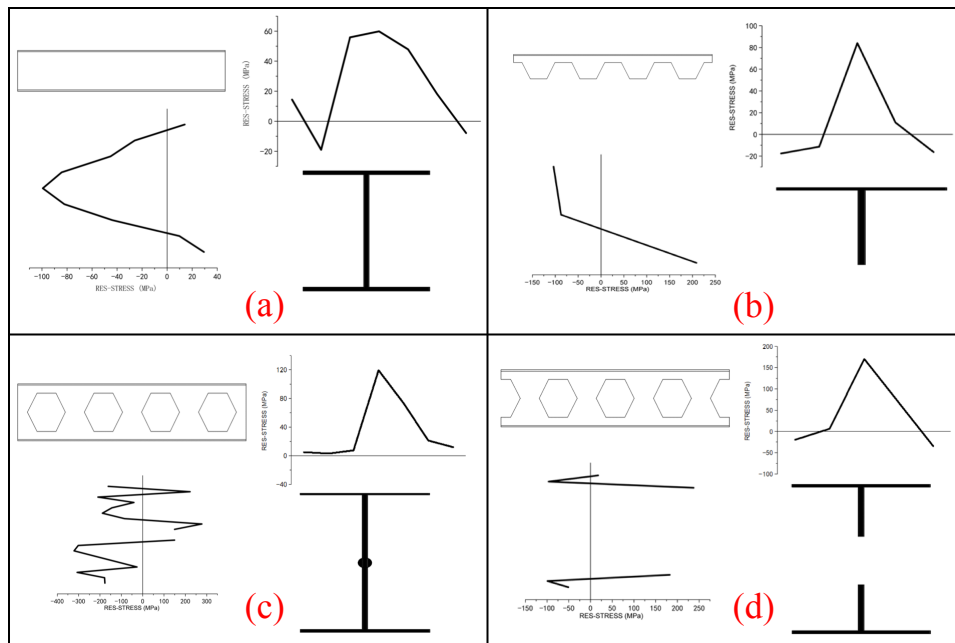


Figure 18: Measured residual stresses of the A-castellated beam: (a) parent section; (2) after flame cutting; (3) web post section after welding; (4) Tee section after welding

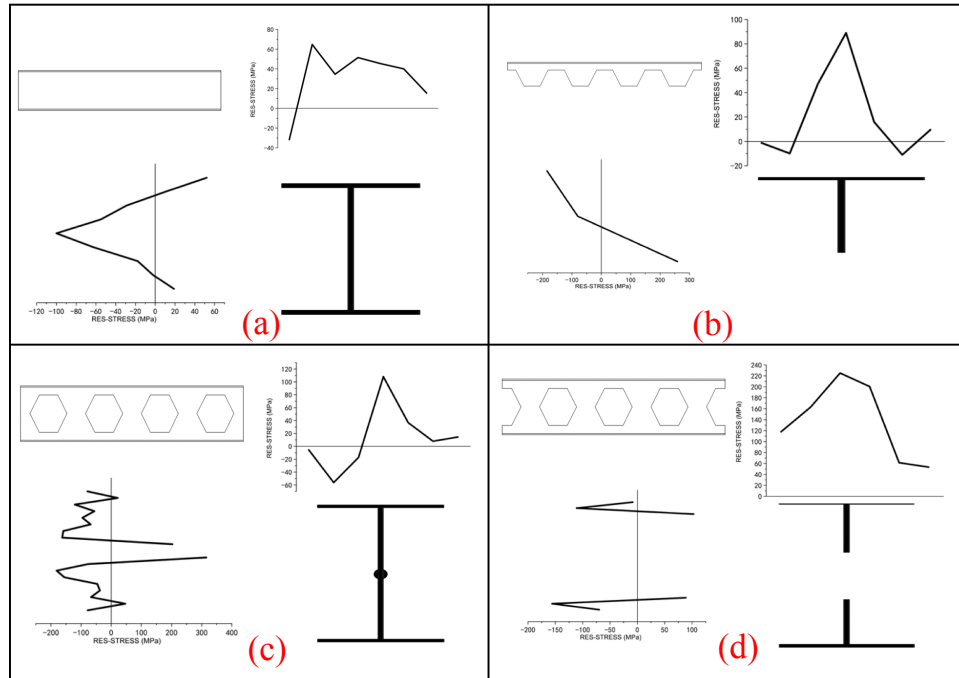


Figure 19: Measured residual stresses of the B-castellated beam: (a) parent section; (2) after flame cutting; (3) continuous web section after welding; (4) Tee section after welding

Computational simulations of this fabrication process have been carried out by the authors in another separated study (Zhou et al. 2018). The thermal residual stresses in the flange are based on the superposition of the thermal residual stresses due to cutting and welding as predicted by the computational models. A proof-of-concept development of the residual stress distribution in the castellated beams is discussed. This new set of experimental data on residual stresses can be further used to validate the proposed residual stress pattern for design recommendations, especially these are closely tied to the castellated beams that could be subjected to distortional buckling failure.

4. Conclusions

The potential distortional buckling failure of castellated beam can be complicate, especially with the coupling of the lateral and local buckling. The paper presents the experimental results of castellated beams experiencing the distortional buckling failure and provides the experimental measurement of the related residual stresses. All the tested castellated beams clearly demonstrate the distortional buckling failure once reaching the critical load. By comparing the tested beam strengths with AISC strength, the value of the moment gradient factor C_b from tests is below the AISC specified for this particular loading case. Hence, reduction in the C_b value needs to be considered for castellated beams failed by lateral-distortional buckling due to the web distortion. Furthermore, the residual stresses are measured in the tested castellated member specimens and their parent sections. These measured residual stresses not only show the distribution for these particular sections but also could be used to validate the computational models of simulating the thermal residual stresses previously developed by the author, hence enable more parametric studies for the development of the residual stress pattern for castellated beams for design recommendations subjected to distortional buckling.

Future work

The data set of the experimentally measured residual stresses can be used for the validation of the computational model for simulating residual stresses of castellated beams, thus enabling a comprehensive parametric study to develop the residual stress pattern in castellated beams that may be experiencing distortional buckling. In addition, as future work, a developed nonlinear finite element model considering initial geometric imperfection and the modified residual stress pattern of castellated beams, can be validated by comparing its results with the experimental results obtained by these bending tests on castellated beams failed by distortional buckling. Finally, a comprehensive parametric study based on the developed model will be carried out to investigate the effect of residual stresses on the distortional buckling resistance of castellated beams, as well as to modify the theoretical expressions for predicting the distortional buckling loads of castellated beams accounting for the residual stresses, the torsional and warping rigidities reductions due to the web distortion.

Acknowledgments

The authors are grateful for the financial support provided by the National Key R & D Program of China (Grant No. 2016YFC0701201), by the National Natural Science Foundation of China (Grant No. 51508051) and by the Fundamental Research Funds for the Central Universities (Grant No. 106112015CDJXY200009).

References

- AISC (2010). Specification for structural steel buildings, *American institute for steel construction, ANSI/AISC 360-10*.
- Altfillisch, M.D., Cooke, B.R. & Toprac, A.A. (1957). An investigation of open web expanded beams. *Welding research council bulletin*, 47, pp.77–88.
- Bradford, M.A. (1992). Lateral-Distortional buckling of steel I-Section members. *Journal of Constructional Steel Research*, 23(1), pp.97–116.
- Ellobody, E. (2011). Interaction of buckling modes in castellated steel beams. *Journal of Constructional Steel Research*, 67(5), pp.814–825.
- El-Sawy, K.M., Sweedan, A.M.I. & Martini, M.I. (2014). Moment gradient factor of cellular steel beams under inelastic flexure. *Journal of Constructional Steel Research*, 98, pp.20–34.
- GB/T11263-2010 (2010). Hot-rolled H and cut T section steel. *China: The People's Republic of China General Administration of Quality Supervision, Inspection and Quarantine*.
- Husain, M.U. & Speirs, W.G. (1973). Experiments on castellated steel beams. *Journal of American Welding Society, Welding Research Supplement*, 52(8), pp.329–342.
- Kalkan, I. & Buyukkaragoz, A. (2012). A numerical and analytical study on distortional buckling of doubly-symmetric steel I-beams. *Journal of Constructional Steel Research*, 70, pp.289–297.
- Kerdal, D. & Nethercot, D.A. (1984). Failure modes for castellated beams. *Journal of Constructional Steel Research*, 4(4), pp.295–315.
- Mohebbkhah, A. (2004). The moment-gradient factor in lateral-torsional buckling on inelastic castellated beams. *Journal of Constructional Steel Research*, 60(10), pp.1481–1494.
- Nethercot, D.A. & Kerdal, D. (1982). Lateral-torsional buckling of castellated beams. *The Structural Engineer*, 60B(3), pp.53–61.
- Pi, Y.L. & Trahair, N.S. (2000). Distortion and warping at beam supports. *Journal of Structural Engineering, ASCE*, 126, pp.1279–1287.
- Showkati, H. et al. (2012). Experiments on elastically braced castellated beams. *Journal of Constructional Steel Research*, 77, pp.163–172.
- Sonck, D. (2014). Global buckling of castellated and cellular steel beams and columns. *Ghent University*. Ph.D. thesis
- Sweedan, A.M.I. (2011). Elastic lateral stability of I-shaped cellular steel beams. *Journal of Constructional Steel Research*, 67(2), pp.151–163.

- Toprac, A.A. & Cooke, B.R. (1959). An experimental investigation of open-web beams. *Welding research council bulletin*, 47, pp.1–10.
- Zaarour, W. & Redwood, R. (1996). Web buckling in thin webbed castellated beams. *Journal of Structural Engineering, ASCE*, 122(8), pp.860–866.
- Zhou, X., Li, J., He, Y., He, Z., Li, Z. (2018). Finite element analysis of thermal residual stresses in castellated beams. *Journal of Constructional Steel Research*, 148, pp.741–755.
- Zirakian, T. (2008). Elastic distortional buckling of doubly symmetric I-shaped flexural members with slender webs. *Thin-Walled Structures*, 46(5), pp.466–475.
- Zirakian, T. & Showkati, H. (2006). Distortional buckling of castellated beams. *Journal of Constructional Steel Research*, 62(9), pp.863–871.
- Zirakian, T. & Showkati, H. (2007). Experiments on distortional buckling of I-beams. *Journal of Structural Engineering, ASCE*, 133(7), pp.1009–1017.